Journal of the Optical Society of America B
OPTICAL PHYSICS

Extreme ultraviolet transient absorption of solids from femtosecond to attosecond timescales [Invited]

Lauren J. Borja,[1] M. Zürch,[1] C. D. Pemmaraju,[2,3] Martin Schultze,[1,5] Krupa Ramasesha,[1,6] Andrey Gandman,[1,7] James S. Prell,[1,8] David Prendergast,[2] Daniel M. Neumark,[1,3] and Stephen R. Leone[1,3,4,*]

[1]Department of Chemistry, University of California, Berkeley, California 94720, USA
[2]The Molecular Foundry, Lawrence Berkeley National Laboratory, Berkeley, California 94720, USA
[3]Chemical Sciences Division, Lawrence Berkeley National Laboratory, Berkeley, California 94720, USA
[4]Department of Physics, University of California, Berkeley, California 94720, USA
[5]Current Address: Fakultät für Physik, Ludwig-Maximilians-Universität, Am Coulombwall 1, D-85748 Garching, Germany
[6]Current Address: Combustion Research Facility, Sandia National Laboratories, Mail Stop 9055, Livermore, California 94551-0969, USA
[7]Current Address: Solid State Institute, Technion–Israel Institute of Technology, Haifa, 32000, Israel
[8]Current Address: Department of Chemistry and Biochemistry, University of Oregon, Eugene, Oregon 97403, USA
*Corresponding author: srl@berkeley.edu

Received 29 February 2016; revised 28 March 2016; accepted 29 March 2016; posted 30 March 2016 (Doc. ID 260159); published 26 April 2016

High-harmonic generation (HHG) produces ultrashort pulses of extreme ultraviolet radiation (XUV), which can be used for pump–probe transient absorption spectroscopy in metal oxides, semiconductors, and dielectrics. Femtosecond transient absorption on iron and cobalt oxides identifies ligand-to-metal charge transfer as the main spectroscopic transition, rather than metal-to-metal charge transfer or d–d transitions, upon photoexcitation in the visible. In silicon, attosecond transient absorption reveals that electrons tunnel into the conduction band from the valence band under strong-field excitation, to energies as high as 6 eV above the conduction band minimum. Extensions of these experiments to other semiconductors, such as germanium, and other transition metal oxides, such as vanadium dioxide, are discussed. Germanium is of particular interest because it should be possible to follow both electron and hole dynamics in a single measurement using transient XUV absorption.

OCIS codes: (190.4160) Multiharmonic generation; (300.6470) Spectroscopy, semiconductors; (320.7130) Ultrafast processes in condensed matter, including semiconductors.

http://dx.doi.org/10.1364/JOSAB.33.000C57

1. INTRODUCTION

Highly nonlinear interactions between intense laser pulses and noble gas media have led to the creation of high-order harmonics [1], largely due to the advances of femtosecond laser technology [2]. Importantly, high-harmonic generation (HHG) has led to the creation of femtosecond and attosecond pulses in the extreme ultraviolet (XUV) with a spectral bandwidth spanning up to tens of electron volts, allowing attosecond pulse production [3]. Extreme ultraviolet light is resonant with core level transitions, which are well separated for individual elements, compared to transitions in the optical or near-infrared (NIR) regions. As has been demonstrated at synchrotron x-ray sources with longer pulses, core level spectroscopy provides element, oxidation [4], and spin [5] state specificity. High-harmonic XUV pulses are ultrashort in duration and this combined with core-level specificity make them ideal probes for unraveling dynamics in the solid state.

Because the emitted XUV radiation generated by HHG is intrinsically phase locked to the driving pulse, establishing various pump–probe experimental schemes is readily realized. The broadband spectral distribution of the XUV pulse is used as a high-temporal-resolution probe, which can be used to excite or probe a wide range of core state transitions in atoms, molecules, and solids. XUV photoelectron spectroscopy has been performed with HHG on atoms [3], molecules [6], and solids [7,8], and all-optical detection pump–probe experiments have also been established, with transient absorption being the most ubiquitous. In the gas phase, XUV transient absorption experiments have been used extensively in the femtosecond [9,10] and attosecond [11,12] regimes, and such experiments have been reviewed elsewhere [13–15]. Transient reflectivity experiments have also been developed to monitor magnetization dynamics [16,17]. This article focuses on XUV transient absorption in solids using femtosecond and attosecond sources as probes. In the experiments discussed in this paper, optical or NIR light excites carriers in metal oxides, dielectrics, or semiconductor materials, and the ensuing dynamics are traced

by typically probing a core-level M- or L-edge absorption using a time-delayed XUV pulse; excitation of N- and O- levels with existing HHG pulses is also possible. First, a brief summary of ultrafast dynamics in solids is considered, followed by a discussion of the experimental considerations for undertaking transient absorption experiments. Several femtosecond and attosecond transient absorption results are then reviewed, and future directions for the field are presented.

2. CARRIER EXCITATION IN SEMICONDUCTORS

The observation of electronic processes that occur in solids after ultrafast excitation has been a goal of picosecond [18], femtosecond [19–25], and now attosecond [15,26,27] spectroscopy. Semiconductors, metal oxides, and even metals form the basis of many photovoltaic and transistor devices, and an understanding of charge separation and migration in these materials can provide more informed design and increased efficiency, which motivates these ultrafast experiments. Upon interaction with an ultrafast near-infrared (NIR) or optical pulse, carriers are excited to non-equilibrium distributions in the valence and conduction band. Considering specific materials of interest, semiconductors and transition metal oxides are used as photocatalysts [28], photovoltaics [29–31], and components in transistor devices [32] primarily because of their tunable bandgaps in the visible and charge carrier separation properties, as well as their high natural abundance and stability [29,33]. Silicon transistors remain ubiquitous in computing devices and detectors, while III–V compounds are frequently used in photovoltaic devices and light-emitting diodes [30,31]. The bonding in transition metal oxides is more ionic in nature than the covalent bonding of semiconductors like silicon, germanium, and gallium arsenide, giving rise to both catalytic and semiconductor-like properties. Many transition metal oxides also exhibit strong electronic correlations that drive reversible changes in physical properties, such as insulator to metal transitions, responsive to pressure, temperature, or dopant concentration. Important questions remain as to whether the transitions are driven by purely electronic processes (Mott) or whether electron–phonon interactions (Peierls) are important [32]. Further understanding of hot carrier relaxation can inform these mechanistic debates while potentially contributing to the development of novel field effect transistor devices, as well [34].

Immediately following carrier excitation, momentum randomization takes place via carrier–carrier and carrier–phonon scattering. Within the first tens [19] to hundreds [20,21,23,35] of femtoseconds, a carrier distribution that is described by an elevated Fermi–Dirac temperature forms. Observation of these initial fast processes, often driven by electron correlation, compels the use of state-of-the-art ultrafast experiments. After an initial hot carrier energy redistribution, continued scattering with phonons brings the lattice temperature into equilibrium with the carrier distribution, over tens to hundreds of picoseconds. Finally, carrier recombination processes, such as direct or Auger recombination [18,36,37], return the system to its initial state. Disentangling carrier–carrier and carrier–phonon scattering has been of interest for many decades. The two-temperature model simply assigns separate electron and phonon relaxation timescales [38]; extending this model [39] or developing new models based on quantum kinetics [40,41] is needed. Control of the electron–phonon scattering [42], carrier inversion [43], and coherent phonon oscillations [44,45] have all been observed and explained within newer quantum frameworks. Spectroscopy with the shortest possible light pulses holds promise to continue to shed light on the evolution of various relaxation and recombination pathways.

3. EXPERIMENTAL CONSIDERATIONS FOR SOLID-STATE EXPERIMENTS WITH HHG

Extreme ultraviolet light from 30 to 300 eV and even higher [46] can be produced with table-top sources. The XUV pulses generated via HHG are now routinely used to study metals [7,8], semiconductors [27], dielectrics [26], and transition metal oxides [24,25] in addition to gases [10–12,47,48]. Although the conversion efficiency is low, HHG sources offer additional advantages over traditional XUV sources, such as synchrotrons, in that the emitted radiation is intrinsically locked in time to the generating laser pulse and pulses as short as 67 as in duration can be produced [49]. The pulse pairs, one in the NIR and one in the XUV, can thus be readily used in ultrafast pump–probe schemes such as transient absorption (Fig. 1), providing time resolution of femtoseconds and even attoseconds. In a typical transient absorption experiment in solids, a NIR or optical pulse is used to excite carriers in the sample, and the XUV attosecond pulse train or isolated attosecond pulse is used as a broadband probe in absorption. By varying the conditions for HHG, the probe can sample the band edges of different elements, such as silicon, iron, cobalt, and germanium. The relatively small number of XUV photons (conversion efficiencies of 10^{-6} for isolated attosecond pulses [50] and 10^{-4} for XUV pulse trains [51], although an efficiency of 10^{-4} has been reported for isolated attosecond pulses, as well [52]) is sufficient for transient absorption experiments when coupled with a stronger NIR or optical pulse. The relatively weak XUV flux ensures that the XUV probe pulses will not induce significant carrier redistribution themselves. Complications arise, however, in the overlap of the XUV and NIR pulses due to the AC Stark effect and phase shifts imparted by coupling to nearby states [53]. In contrast to gas-phase experiments where core–hole lifetimes of tens of femtoseconds [54,55] modify the observed pump–probe time-delay-dependent changes, in solids, screening and dephasing of the core hole happens much faster, on a timescale of 1 fs [56]. This rapid response makes these transitions suitable for probing ultrafast charge transfer dynamics.

Figure 1 is a schematic of a HHG pump–probe apparatus. A beam splitter (BS) is used to divide the femtosecond pulse into a pump and probe arm. The probe arm (bottom) is focused using a focusing mirror (FM1) into the HHG cell,

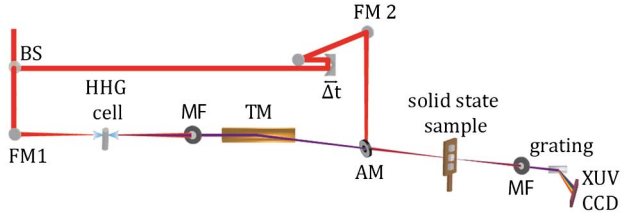

Fig. 1. Schematic representation of a HHG XUV transient absorption experimental apparatus.

which contains the nonlinear medium used to generate the broadband XUV probe. The residual NIR light is blocked with a metallic filter (MF), and a toroidal mirror (TM) focuses the XUV probe through the hole in the annular mirror (AM) onto the solid-state sample. The pump arm (top) is sent onto mirrors mounted on piezoelectric translational stages to precisely control the time delay (Δt). The pump is then focused with a focusing mirror (FM2) onto an annular mirror (AM) for collinear recombination with the pump pulse. After transmitting through the sample, the remaining pump NIR light is blocked with a second metal filter and the XUV light is dispersed with a flat-field grating onto an XUV CCD camera.

For solid-state transient absorption experiments, ultrathin samples must be used. Many materials have attenuation lengths, or the distance at which the intensity of the XUV is reduced to $1/e = 36.8\%$ of the incident light, of 10–50 nm at 100 eV [57], meaning that solid-state samples for XUV transient absorption should be of that order of magnitude of thickness for use in table-top experiments. Moreover, the index of refraction difference between optical wavelengths and XUV radiation leads to a temporal slip in transmission experiments between the two in thick samples. While some free-standing samples are available for XUV transient absorption measurements (e.g., silicon dioxide [26] and silicon [27]), for many materials it is difficult to produce free-standing samples thinner than hundreds of nanometers. Instead, it is possible to deposit such materials on ultrathin membranes such as silicon nitride for support. This is especially true for composite materials, such as transition metal oxide semiconductors or materials with morphology-dependent structural properties.

As a versatile support material, thin silicon nitride membranes, 30–100 nm thick, have been used in both XUV [24,25,58] and x-ray [59,60] transient absorption experiments. Thin films and free-standing samples pose additional experimental challenges, as they have low thermal conductivity compared to bulk samples [61], and often the NIR or optical intensities desired to induce a particular process are at or close to the damage thresholds of these submicrometer thick samples [62]. To excite a strong field process the flux must be high, but often this is done at a nonresonant frequency, and the process is adiabatic [26]. Excitation at a resonance can excite carriers at lower field intensities, but then increased absorption of the pump occurs and, consequently, sample damage can also result.

As noted, another consideration for attosecond resolution is the vastly different indices of refraction of the NIR and XUV pulses in the solid sample. The NIR or optical excitation pulse typically has a much larger index of refraction for a semiconductor or transition metal oxide sample [63], compared to the index for the XUV [57]. Hence, the XUV pulse averages over a range of NIR or optical pulse electric field phases. In very thin samples, the XUV probe signal follows the half-cycles of the driving laser fields in solids [26,27,64], and to observe these fast modulations of optical properties in a transient absorption experiment, it is necessary to keep the phase slip to less than a half-cycle of NIR or optical light. An upper bound for thin film thickness, d, for a central frequency of the pump, λ_{NIR}, in nanometers, is

$$d\ [\mathrm{nm}] \leq \frac{1}{2}\frac{\lambda_{\mathrm{NIR}}}{n_{\mathrm{NIR}} - n_{\mathrm{XUV}}}, \tag{1}$$

where n_{NIR} and n_{XUV} are the indices of refraction of the NIR and XUV in the material, respectively. For an experiment in silicon with a NIR pump at 1.5 eV probed using the $L_{2,3}$-edge at 100 eV, which has n_{NIR} (1.5 eV) = 3.673 and n_{XUV} (100 eV) = 1.03, the maximum allowed thickness is ∼150 nm. As a comparison, an experiment in germanium with a NIR pump at 1.5 eV probed using the $M_{4,5}$-edge at 30 eV, n_{NIR} (1.5 eV) = 4.653 and n_{XUV} (30 eV) = 0.95, would require samples thinner than ∼105 nm. All index of refraction data are taken from [63].

4. FEMTOSECOND TRANSIENT ABSORPTION EXPERIMENTS

The interesting band structure of transition metal oxides arises primarily because the partially filled d orbitals of the transition metal can take on a different bonding character when bound to oxygen. Bonding and antibonding orbitals are formed by a combination of the d atomic orbitals of the transition metal and the $2p$ atomic orbitals of oxygen. Between these, however, lie the nonbonding d orbitals of the transition metal oxide, which are themselves partially filled. This allows for three different types of electronic charge transfer transitions: metal-to-metal, metal-to-ligand, and ligand-to-metal charge transfer. In the metal-to-metal charge transfer process (MMCT), an electron moves from a filled to an empty nonbonding d orbital on a different metal atom. In a metal-to-ligand charge transfer process (MLCT), the electron instead transfers from the metal to an orbital with more ligand character, such as the antibonding orbitals between the transition metal and the oxygen. A third pathway for optical excitation is the ligand-to-metal charge transfer (LMCT), where the electron transfers from an orbital of ligand character to an empty d orbital on the metal [65]. These orbitals form the basis of the extended band structure in the bulk. The existence of so many transitions complicates the assignment of transitions in the visible and ultraviolet spectra of transition metal oxides; disentangling such transitions from one another has been addressed by various electronic structure calculations [66–70]. Experimentally, the assignments can be obtained via x-ray or XUV transient absorption spectroscopy [71,72].

In iron oxide, many electronic structure calculations have offered competing assignments of the transitions in the ultraviolet and visible spectrum. The visible spectrum of α-iron oxide shows peaks at both 2.2 and 3.2 eV [67,68], and theory is unable to reach a consensus on the nature of these two transitions [66–68]. Calculations initially assigned the energetically lower feature in the visible spectrum to a d–d spin allowed transition within iron ions and the energetically higher feature to a LMCT state between the oxygen and the iron [66]. Other calculations found the LMCT state to be the lower energy state [67], conflicting with the earlier work. To correctly assign these transitions, a probe with oxidation specificity is needed; a reduction of the iron ion occurs in the LMCT but not in the d–d transition, making a clear distinction.

The transition metal oxides are good candidates for XUV transient absorption, because many transition metals have M-edge absorption features from 30–70 eV, a range accessible with current HHG technology. With a table-top HHG instrument [Fig. 1(a)], XUV transient absorption spectroscopy,

coupled with semi-empirical ligand field multiplet calculations [73], identified the nature of the charge transfer after photoexcitation at 3.1 eV (400 nm) [19] in α-iron oxide, also known as hematite. For solid-state XUV transient absorption spectroscopy, 14 nm thick α-iron oxide was deposited onto a 100 nm thick silicon nitride substrate. High harmonics from 45 to 70 eV are well centered about the iron $M_{2,3}$-edge at 57 eV, corresponding to an excitation from the iron $3p$ core state. An excited state is formed immediately after interaction with the 3.1 eV pulse, whose differential optical density is shown as the black line in Fig. 2. The differential optical density of the excited state is compared to two different differential optical densities simulated using the CTM4XAS55 program [73], and the LMCT state (blue line in Fig. 2) is in excellent agreement. The simulated d–d transition (red line in Fig. 2) does not match the excited state, supporting one of the previous calculations [67].

In a similar experiment, the charge transfer state in spinel cobalt oxide at 3.1 eV was also assigned [25]. Because of the spinel structure, the cobalt atoms exist in mixed-valence cobalt (II) or (III) oxidation states. This gives rise to a wealth of possible charge transfer pathways, where an electron can transfer from the oxygen to either of the cobalt ions (LMCT), between cobalt ions (MMCT), or within each cobalt ion (d–d transition). The initial state best matches the simulated LMCT from the oxygen anion to the cobalt (III) cation. This state then decays in amplitude within 190 fs, while shifting to lower energies over 535 fs. The 190 fs decay in amplitude is also intensity dependent, increasing at higher excitation density. This intensity-dependent decay rate could indicate Auger relaxation, while the slower spectral shift over 535 fs may be related to hot carrier–phonon scattering.

5. ATTOSECOND TRANSIENT ABSORPTION EXPERIMENTS

After the first attosecond transient absorption experiment in a solid was performed on a dielectric, silicon dioxide [26], a seminal transient absorption experiment in a semiconductor, silicon [27], tracked carrier excitation after ultrashort laser pulse excitation and the resulting band structure modifications. The attosecond transient absorption experiment was performed on free-standing 140–250 nm thick single crystal silicon membranes in the ⟨100⟩ orientation [27]. The sample was excited with 4 fs carrier–envelope phase (CEP)-stabilized NIR laser pulses comprising spectral components with photon energies between 1.1 and 2.7 eV [Fig. 3(a)]. These intense few-cycle pulses promote up to 1% of all the valence band electrons into the conduction band and significantly alter the band structure of silicon. Probing of the conduction band modifications is achieved with attosecond pulses centered around the $L_{2,3}$-edge of silicon at 99 eV, corresponding to a $2p$ core transition [Fig. 3(b)]. The experiments allowed identification of the electron excitation mechanism and tracked the resulting conduction bandgap shift that is found to occur before the fastest optical phonon is excited. By comparing the excited-state experimental spectra to state-of-the-art calculations of the silicon $L_{2,3}$-edge coupled with time-dependent density functional theory (TD-DFT) [74,75], these effects can be disentangled.

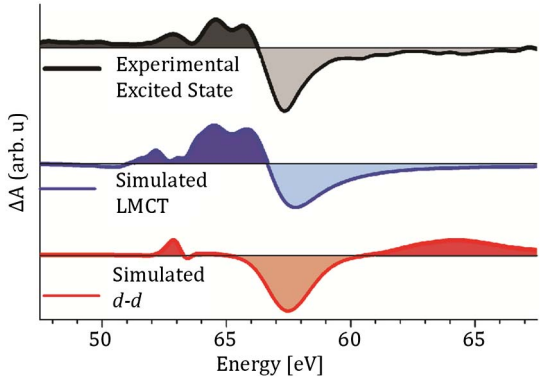

Fig. 2. Differential optical density (ΔA) for the LMCT state (red) and d–d transition state (blue), which were compared to the experimentally observed excited state differential absorption (black). The experimentally observed state matches the simulated LMCT state, while bearing little resemblance to the simulated differential absorption for the d–d transition. Reprinted with permission from Vura-Weis *et al.*, J. Phys. Chem. Lett., **4**, 3667–3671 (2013) [24]. Copyright 2013 American Chemical Society.

At intensities of 10^{12} W/cm^2 the experiment in tandem with TD-DFT computations finds that electrons are promoted across the bandgap via tunneling to reach states more energetic in the conduction band than if excited via multiphoton coupling by the NIR pulse across the indirect band gap. This excitation mechanism excites up to 1% of the valence electrons before sample damage occurs due to the extremely short pump duration. Broadening of the $L_{2,3}$-edge features are observed that extend to 6 eV above the edge onset [Fig. 4(a)], which TD-DFT calculations showed to be evidence of the strong-field tunneling mechanism. Half-cycle steps are visible in the transmission at the band edge of silicon [Fig. 4(b)]. Error function fits to individual steps extract a time duration for the electronic response of <450 as [inset, Fig. 4(b)]. Assuming the electrons tunnel instantaneously in the presence of the field [64,76,77], it appears that their arrival in the conduction band rather immediately affects the core-level electron transition. The observed step rise time places an upper bound on the time it takes for the excited state to affect the XUV absorption, which is considered a many-body carrier scattering response to a core electron transition.

Additionally, broadening of the entire silicon $L_{2,3}$-edge occurs and persists beyond the 200 fs time period measured in this experiment. Looking at the derivative of the XUV absorption versus time, the sharp features existing at negative time delays decrease in amplitude and broaden spectrally. The time evolution of the differential absorption at 100.2 eV shows a biexponential-like decay [Fig. 4(c)]. The initial sharp decrease occurring within $\tau_e = 5$ fs is indicative of the fast rate of electronic relaxation that occurs before the onset of lattice dynamics. An additional 20% broadening over the remaining time delays has a timescale of $\tau_p = 60$ fs. The 60 fs decay matches the period of the fastest optical phonon [44,45], which is coherently excited by the electronic response due to the few-cycle pulse. During this lattice motion, the ion cores in the silicon lattice are displaced a distance of 6 pm from their initial equilibrium positions, according to calculations that estimate the spectral changes that correspond to the observed additional 20% broadening of the silicon $L_{2,3}$ edge. The results support

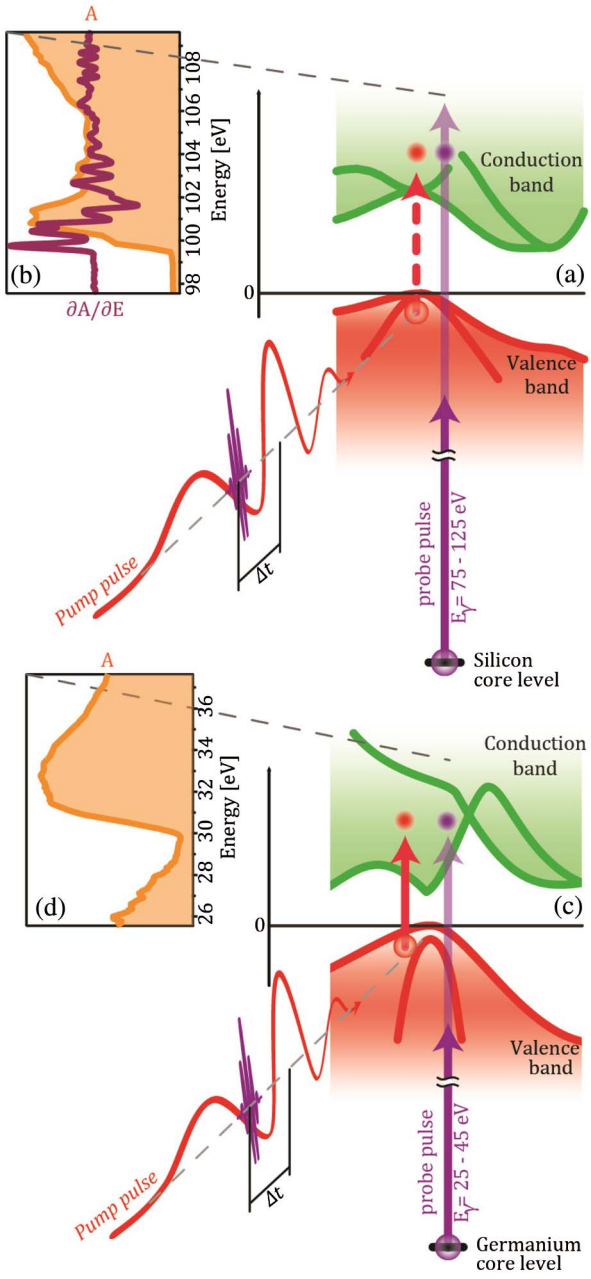

Fig. 3. (a) In silicon, electrons excited into the conduction band alter (b) the XUV absorbance (A) and differential absorbance ($\partial A/\partial E$) of the silicon $L_{2,3}$-edge at 100 eV. (c) In germanium, electrons excited into the conduction band of germanium alter (d) the XUV absorbance (A) of the germanium $M_{4,5}$-edge at 30 eV. Adapted from [27].

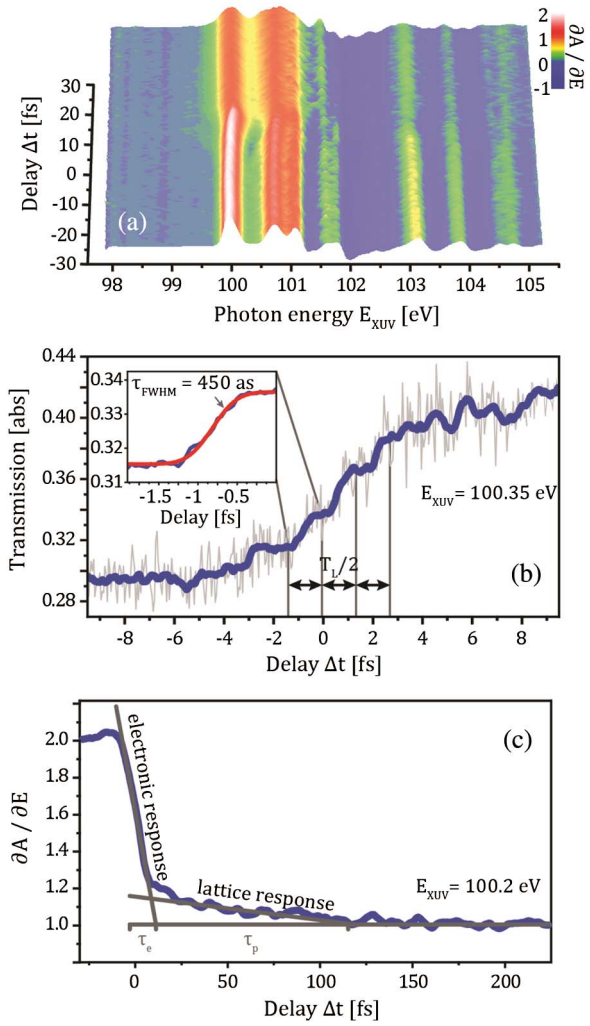

Fig. 4. (a) The differential absorbance, ($\partial A/\partial E$), versus time delay over the silicon $L_{2,3}$-edge. (b) Sub-cycle steps in the transmission at the band edge of silicon, shown with (inset) a 450 as error function fit to a single step. (c) The biexponential decay of the differential data, showing a separation of electronic and lattice dynamics. From Schultze *et al.*, Science, **346**, 1348–1352 (2014) [27]. Reprinted with permission from AAAS.

that the features occurring at later times correspond to the response to the onset of coherent phonon motion. Recurrences due to coherent phonon motion were not observed, but future work is desirable to search for such motion and to determine whether it is observable in XUV absorption.

Out to 200 fs, no further changes were observed, and a study of further time dynamics remains an open goal of XUV transient absorption. A previous time-resolved photoelectron experiment in silicon [20] reported that the electron–electron thermalization temperature, the time for electrons to form a distribution described by an elevated electronic temperature that is greater than the temperature of the lattice, occurs in less than an experimental resolution of 120 fs [20]. Moreover, femtosecond pump–probe reflectivity experiments revealed an electron thermalization in the conduction band that occurs within 32 fs followed by a 260 fs electron–phonon relaxation time [23]. Coherent phonon oscillations have also been observed in silicon, with a period of 64 fs, which persist for several picoseconds even at room temperature [44,45]. Further XUV transient absorption experiments at longer time delays need to be performed to characterize how these effects manifest themselves.

6. FUTURE DIRECTIONS FOR XUV TRANSIENT ABSORPTION

In the attosecond transient absorption experiment in silicon, the primary mechanism for carrier excitation was tunneling, because

of the intense few-cycle excitation pulse. However, for different materials, such as gallium arsenide [43] or germanium, single photon excitation at lower intensities is possible. In single-photon absorption, electrons are excited to a narrower region of the conduction band and excess energies may be more straightforward to interpret. Because the carriers are concentrated in a discrete region of the band structure, their effect on the XUV absorption may be analyzed more completely. Hence, it is more likely that effects such as Pauli blocking of the XUV transition may be observed in the one-photon limit.

Electrons are also not the only carrier of interest in bandgap materials. Holes are also created in the valence band, and their presence was not detected in the XUV transient absorption experiments in either silicon dioxide [26] or silicon [27]. In silicon the $L_{2,3}$-edge is a transition from a $2p$ core state, and the valence band in silicon is primarily of $3p$ character, leading to a weak oscillator strength for a transition from the $2p$ core state to the valence band, if it were partially occupied by holes. X-ray photoelectron emission spectroscopy (XES) from the silicon $L_{2,3}$-edge measures the density of states in the valence band, and this, coupled with x-ray absorption spectroscopy, can provide a more complete picture of the bandgap dynamics [78].

Another approach is to find a material for which XUV transient absorption reports on both the conduction and valence band dynamics, such as germanium. While germanium is an indirect bandgap material, it also has a direct bandgap of 0.805 eV at room temperature [79]. Photons with energies of 1.5 eV emitted from a typical titanium–sapphire laser source have sufficient energy to promote electrons into the conduction band with excess energy. An example of a NIR pump–XUV-probe experiment in germanium is shown in Fig. 3(c). The XUV probe would be centered about the $M_{4,5}$-edge of germanium, which lies at 29.5 eV [Fig. 3(d)] and is a transition from the $3d$ core level. As the valence band in germanium is primarily of $4p$ character, a transition from the $3d$ core state to the valence band is dipole allowed if the valence band is not completely filled. The ground-state XUV absorption edge of materials is a transition from the core level to the empty conduction band density of states, with no sensitivity to the completely filled valence band density of states. However, after pump excitation, the available states in the conduction band decrease, reducing the XUV absorption signal [26], and holes in the valence band open up new transitions from the core level. The magnitude of the changes in the XUV absorption is governed by the oscillator strengths of the core transition to the valence and conduction bands. In germanium it should be possible to observe whether, upon carrier excitation, the conduction band decrease occurs with an increase of the valence band after ultrafast excitation [78]. Observation of both the conduction and valence band dynamics simultaneously would yield direct insight into this mechanism.

Theoretical simulations of the density of states weighted by the germanium $M_{4,5}$-edge oscillator strengths enable a comparison between the expected strength of the XUV transitions to the valence and conduction bands of germanium. Considering the calculated oscillator strengths of the $3d$ core state excitations [Fig. 5(a)], which are broadened due to spin–orbit effects, the values sharply increase on both sides of the Fermi edge, indicating that a signal from the holes would indeed be visible in an ultrafast experiment. Because the hole and electron features will occur in different spectral regions, they can be tracked simultaneously in real time. To corroborate this, core-level absorption spectra were simulated for the germanium $M_{4,5}$-edge, including 1% electron-hole doping, and compared to the undoped case [Fig. 5(b)]. The calculations shown in Fig. 5 were carried out within the independent particle approximation and neglecting excitonic effects, the latter of which are expected to be weak in germanium. The electron-hole doping was simulated within the occupation-constrained DFT approach [80]. It is clear that the doped and undoped spectra show distinct differences, with the doped case indicating a clear enhancement of absorbance on the valence band side due to the presence of holes. A concomitant reduction of the intensity on the conduction band side is also expected in a different spectral region due to the presence of change in conduction band electrons.

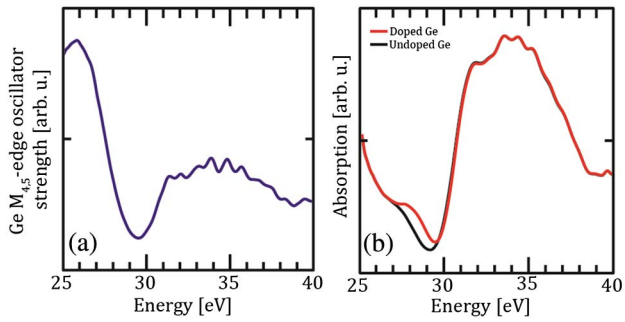

Fig. 5. (a) The germanium $M_{4,5}$-edge oscillator strength shows a distinct increase below 29.5 eV, indicating increased sensitivity to changes in the valence band. (b) Simulated germanium $M_{4,5}$-edge absorption spectra for the undoped (black) and 1% electron and hole doped (red) case.

7. CONCLUSION

In summary, using XUV transient absorption to investigate solid-state materials, electron dynamics in metals, semiconductors and dielectrics are obtained with unprecedented temporal and spectral resolution. Because processes such as electron–electron scattering and electron–phonon scattering occur within the first tens of femtoseconds in many materials, it is necessary to employ methods with attosecond resolution to observe and disentangle these early time competing events. By taking the XUV transitions into account, these measurements give insight into charge-carrier excitation in a spectrally resolved and time-dependent fashion. A combination of ultrafast experiments and sophisticated theory has elucidated the mechanism behind ligand-to-metal charge transfer, electron tunneling, and evidence for separation of purely electronic timescales from slower lattice dynamics. These methods can be extended to investigate electron and hole dynamics and the mechanism of the phase changes in strongly correlated materials in the near future.

Funding. Army Research Office (ARO), Multidisciplinary University Research Initiative (WN911NF-14-1-0383); Multidisciplinary University Research Initiatives from the Air Force Office of Scientific Research (FA9550-15-1-0037); Air Force Office of Scientific Research (AFOSR) (FA9550-14-1-0154);

The Humboldt Foundation; Office of Science (SC); Basic Energy Sciences (BES); U.S. Department of Energy (DOE) (DE-AC02-05CH11231); National Energy Research Scientific Computing Center (NERSC); Lawrence Berkeley National Laboratory; National Security Science and Engineering Faculty Fellowship (NSSEFF) (FA9550-10-1-0195); W.M. Keck Foundation (DE-AC03-76SF00098); National Science Foundation (NSF) (CHE-1361226); Defense Advanced Research Projects Agency (DARPA) (W31P4Q1310017).

Acknowledgment. We acknowledge fruitful discussions with M. F. Jager and C. N. Ott. This work was performed with support from the DARPA PULSE program through a grant from AMRDEC (W31P4Q1310017).

REFERENCES

1. A. McPherson, G. Gibson, H. Jara, U. Johann, T. S. Luk, I. A. McIntyre, K. Boyer, and C. K. Rhodes, "Studies of multiphoton production of vacuum-ultraviolet radiation in the rare gases," J. Opt. Soc. Am. B **4**, 595 (1987).
2. F. X. Kärtner, E. P. Ippen, and S. T. Cundiff, "Femtosecond laser development," in *Femtosecond Optical Frequency Comb: Principle, Operation, and Applications*, J. Ye and S. T. Cundiff, eds. (Springer, 2005), pp. 54–77.
3. M. Hentschel, R. Kienberger, C. Spielmann, G. A. Reider, N. Milosevic, T. Brabec, P. Corkum, U. Heinzmann, M. Drescher, and F. Krausz, "Attosecond metrology," Nature **414**, 509–513 (2001).
4. N. Huse, H. Cho, K. Hong, L. Jamula, F. M. F. de Groot, T. K. Kim, J. K. McCusker, and R. W. Schoenlein, "Femtosecond soft x-ray spectroscopy of solvated transition-metal complexes: deciphering the interplay of electronic and structural dynamics," J. Phys. Chem. Lett. **2**, 880–884 (2011).
5. R. Qiao, T. Chin, S. J. Harris, S. Yan, and W. Yang, "Spectroscopic fingerprints of valence and spin states in manganese oxides and fluorides," Curr. Appl Phys. **13**, 544–548 (2013).
6. F. Calegari, D. Ayuso, A. Trabattoni, L. Belshaw, S. D. Camillis, S. Anumula, F. Frassetto, L. Poletto, A. Palacios, P. Decleva, J. B. Greenwood, F. Martín, and M. Nisoli, "Ultrafast electron dynamics in phenylalanine initiated by attosecond pulses," Science **346**, 336–339 (2014).
7. A. L. Cavalieri, N. Müller, T. Uphues, V. S. Yakovlev, A. Baltuška, B. Horvath, B. Schmidt, L. Blümel, R. Holzwarth, S. Hendel, M. Drescher, U. Kleineberg, P. M. Echenique, R. Kienberger, F. Krausz, and U. Heinzmann, "Attosecond spectroscopy in condensed matter," Nature **449**, 1029–1032 (2007).
8. S. Neppl, R. Ernstorfer, E. M. Bothschafter, A. L. Cavalieri, D. Menzel, J. V. Barth, F. Krausz, R. Kienberger, and P. Feulner, "Attosecond time-resolved photoemission from core and valence states of magnesium," Phys. Rev. Lett. **109**, 087401 (2012).
9. E. R. Hosler and S. R. Leone, "Characterization of vibrational wave packets by core-level high-harmonic transient absorption spectroscopy," Phys. Rev. A **88**, 023420 (2013).
10. M.-F. Lin, D. M. Neumark, O. Gessner, and S. R. Leone, "Ionization and dissociation dynamics of vinyl bromide probed by femtosecond extreme ultraviolet transient absorption spectroscopy," J. Chem. Phys. **140**, 064311 (2014).
11. H. Wang, M. Chini, S. Chen, C.-H. Zhang, F. He, Y. Cheng, Y. Wu, U. Thumm, and Z. Chang, "Attosecond time-resolved autoionization of argon," Phys. Rev. Lett. **105**, 143002 (2010).
12. E. Goulielmakis, Z. H. Loh, A. Wirth, R. Santra, N. Rohringer, V. S. Yakovlev, S. Zherebtsov, T. Pfeifer, A. M. Azzeer, M. F. Kling, S. R. Leone, and F. Krausz, "Real-time observation of valence electron motion," Nature **466**, 739–743 (2010).
13. Z.-H. Loh and S. R. Leone, "Capturing ultrafast quantum dynamics with femtosecond and attosecond x-ray core-level absorption spectroscopy," J. Phys. Chem. Lett. **4**, 292–302 (2013).
14. A. R. Beck, D. M. Neumark, and S. R. Leone, "Probing ultrafast dynamics with attosecond transient absorption," Chem. Phys. Lett. **624**, 119–130 (2015).
15. K. Ramasesha, S. R. Leone, and D. M. Neumark, "Real-time probing of electron dynamics using attosecond time-resolved spectroscopy," Annu. Rev. Phys. Chem., doi: 10.1146/annurev-physchem-040215-112025 (to be published).
16. S. Mathias, C. La-O-Vorakiat, P. Grychtol, P. Granitzka, E. Turgut, J. M. Shaw, R. Adam, H. T. Nembach, M. E. Siemens, S. Eich, C. M. Schneider, T. J. Silva, M. Aeschlimann, M. M. Murnane, and H. C. Kapteyn, "Probing the timescale of the exchange interaction in a ferromagnetic alloy," Proc. Natl. Acad. Sci. USA **109**, 4792–4797 (2012).
17. D. Rudolf, C. La-O-Vorakiat, M. Battiato, R. Adam, J. M. Shaw, E. Turgut, P. Maldonado, S. Mathias, P. Grychtol, H. T. Nembach, T. J. Silva, M. Aeschlimann, H. C. Kapteyn, M. M. Murnane, C. M. Schneider, and P. M. Oppeneer, "Ultrafast magnetization enhancement in metallic multilayers driven by superdiffusive spin current," Nat. Commun. **3**, 1037 (2012).
18. A. Othonos, "Probing ultrafast carrier and phonon dynamics in semiconductors," J. Appl. Phys. **83**, 1789–1830 (1998).
19. P. C. Becker, H. L. Fragnito, C. H. B. Cruz, R. L. Fork, J. E. Cunningham, J. E. Henry, and C. V. Shank, "Femtosecond photon echoes from band-to-band transitions in GaAs," Phys. Rev. Lett. **61**, 1647–1649 (1988).
20. J. R. Goldman and J. A. Prybyla, "Ultrafast dynamics of laser-excited electron distributions in silicon," Phys. Rev. Lett. **72**, 1364–1367 (1994).
21. R. H. M. Groeneveld, R. Sprik, and A. Lagendijk, "Femtosecond spectroscopy of electron-electron and electron-phonon energy relaxation in Ag and Au," Phys. Rev. B **51**, 11433–11445 (1995).
22. F. Rossi and T. Kuhn, "Theory of ultrafast phenomena in photoexcited semiconductors," Rev. Mod. Phys. **74**, 895–950 (2002).
23. A. J. Sabbah and D. M. Riffe, "Femtosecond pump-probe reflectivity study of silicon carrier dynamics," Phys. Rev. B **66**, 165217 (2002).
24. J. Vura-Weis, C.-M. Jiang, C. Liu, H. Gao, J. M. Lucas, F. M. F. de Groot, P. Yang, A. P. Alivisatos, and S. R. Leone, "Femtosecond $M_{2,3}$-edge spectroscopy of transition-metal oxides: photoinduced oxidation state change in α-Fe_2O_3," J. Phys. Chem. Lett. **4**, 3667–3671 (2013).
25. C.-M. Jiang, L. R. Baker, J. M. Lucas, J. Vura-Weis, A. P. Alivisatos, and S. R. Leone, "Characterization of photo-induced charge transfer and hot carrier relaxation pathways in spinel cobalt oxide (Co_3O_4)," J. Phys. Chem. C **118**, 22774–22784 (2014).
26. M. Schultze, E. M. Bothschafter, A. Sommer, S. Holzner, W. Schweinberger, M. Fiess, M. Hofstetter, R. Kienberger, V. Apalkov, V. S. Yakovlev, M. I. Stockman, and F. Krausz, "Controlling dielectrics with the electric field of light," Nature **493**, 75–78 (2012).
27. M. Schultze, K. Ramasesha, C. D. Pemmaraju, S. A. Sato, D. Whitmore, A. Gandman, J. S. Prell, L. J. Borja, D. Prendergast, K. Yabana, D. M. Neumark, and S. R. Leone, "Attosecond band-gap dynamics in silicon," Science **346**, 1348–1352 (2014).
28. M. I. Litter, "Heterogeneous photocatalysis: transition metal ions in photocatalytic systems," Appl. Catal. B **23**, 89–114 (1999).
29. M. C. Toroker and E. A. Carter, "Transition metal oxide alloys as potential solar energy conversion materials," J. Mater. Chem. A **1**, 2474–2484 (2013).
30. A. W. Bett, F. Dimroth, G. Stollwerck, and O. V. Sulima, "III-V compounds for solar cell applications," Appl. Phys. A **69**, 119–129 (1999).
31. M. Bosi and C. Pelosi, "The potential of III-V semiconductors as terrestrial photovoltaic devices," Prog. Photovoltaics Res. Appl. **15**, 51–68 (2007).
32. Z. Yang, C. Ko, and S. Ramanathan, "Oxide electronics utilizing ultrafast metal-insulator transitions," Annu. Rev. Mater. Res. **41**, 337–367 (2011).
33. J. B. Goodenough, "Perspective on engineering transition-metal oxides," Chem. Mater. **26**, 820–829 (2014).
34. Y. Zhou and S. Ramanathan, "Correlated electron materials and field effect transistors for logic: a review," Crit. Rev. Solid State Mater. Sci. **38**, 286–317 (2013).
35. X. Q. Zhou, H. M. van Driel, and G. Mak, "Femtosecond kinetics of photoexcited carriers in germanium," Phys. Rev. B **50**, 5226–5230 (1994).

36. J. Shah, *Ultrafast Spectroscopy of Semiconductors and Semiconductor Nanostructures*, Vol. **115** of Springer Series in Solid-State Sciences (Springer, 1999).
37. S. K. Sundaram and E. Mazur, "Inducing and probing non-thermal transitions in semiconductors using femtosecond laser pulses," Nat. Mater. **1**, 217–224 (2002).
38. S. I. Anisimov, B. L. Kapeliovich, and T. L. Perel'man, "Electron emission from metal surfaces exposed to ultrashort laser pulses," Sov. Phys. J. Exp. Theor. Phys. **39**, 375–377 (1974).
39. E. Carpene, "Ultrafast laser irradiation of metals: beyond the two-temperature model," Phys. Rev. B **74**, 024301 (2006).
40. L. Bányai, D. B. T. Thoai, E. Reitsamer, H. Haug, D. Steinbach, M. U. Wehner, M. Wegener, T. Marschner, and W. Stolz, "Exciton-LO-phonon quantum kinetics: evidence of memory effects in bulk GaAs," Phys. Rev. Lett. **75**, 4335 (1995).
41. W. A. Hügel, M. F. Heinrich, M. Wegener, Q. T. Vu, L. Bányai, and H. Haug, "Photon echoes from semiconductor band-to-band continuum transitions in the regime of coulomb quantum kinetics," Phys. Rev. Lett. **83**, 3313–3316 (1999).
42. M. U. Wehner, M. H. Ulm, D. S. Chemla, and M. Wegener, "Coherent control of electron-LO-phonon scattering in bulk GaAs," Phys. Rev. Lett. **80**, 1992–1995 (1998).
43. Q. T. Vu, H. Haug, O. D. Mücke, T. Tritschler, M. Wegener, G. Khitrova, and H. M. Gibbs, "Light-induced gaps in semiconductor band-to-band transitions," Phys. Rev. Lett. **92**, 217403 (2004).
44. M. Hase, M. Kitajima, A. M. Constantinescu, and H. Petek, "The birth of a quasiparticle in silicon observed in time–frequency space," Nature **426**, 51–54 (2003).
45. M. Hase, M. Katsuragawa, A. M. Constantinescu, and H. Petek, "Frequency comb generation at terahertz frequencies by coherent phonon excitation in silicon," Nat. Photonics **6**, 243–247 (2012).
46. M.-C. Chen, P. Arpin, T. Popmintchev, M. Gerrity, B. Zhang, M. Seaberg, D. Popmintchev, M. M. Murnane, and H. C. Kapteyn, "Bright, coherent, ultrafast soft x-ray harmonics spanning the water window from a tabletop light source," Phys. Rev. Lett. **105**, 173901 (2010).
47. B. Bernhardt, A. R. Beck, X. Li, E. R. Warrick, M. J. Bell, D. J. Haxton, C. W. McCurdy, D. M. Neumark, and S. R. Leone, "High-spectral-resolution attosecond absorption spectroscopy of autoionization in xenon," Phys. Rev. A **89**, 023408 (2014).
48. A. R. Attar, L. Piticco, and S. R. Leone, "Core-to-valence spectroscopic detection of the CH_2Br radical and element-specific femtosecond photodissociation dynamics of CH_2IBr," J. Chem. Phys. **141**, 164308 (2014).
49. K. Zhao, Q. Zhang, M. Chini, Y. Wu, X. Wang, and Z. Chang, "Tailoring a 67 attosecond pulse through advantageous phase-mismatch," Opt. Lett. **37**, 3891–3893 (2012).
50. Z. Chang, *Fundamentals of Attosecond Optics*, 1st ed. (CRC Press, 2011).
51. J.-P. Brichta, M. C. H. Wong, J. B. Bertrand, H.-C. Bandulet, D. M. Rayner, and V. R. Bhardwaj, "Comparison and real-time monitoring of high-order harmonic generation in different sources," Phys. Rev. A **79**, 033404 (2009).
52. E. J. Takahashi, P. Lan, O. D. Mücke, Y. Nabekawa, and K. Midorikawa, "Attosecond nonlinear optics using gigawatt-scale isolated attosecond pulses," Nat. Commun. **4**, 2691 (2013).
53. S. Pabst, A. Sytcheva, A. Moulet, A. Wirth, E. Goulielmakis, and R. Santra, "Theory of attosecond transient-absorption spectroscopy of krypton for overlapping pump and probe pulses," Phys. Rev. A **86**, 063411 (2012).
54. J. L. Campbell and T. Papp, "Widths of the atomic K–N7 levels," At. Data Nucl. Data Tables **77**, 1–56 (2001).
55. C. Nicolas and C. Miron, "Lifetime broadening of core-excited and-ionized states," J. Electron. Spectrosc. Relat. Phenom. **185**, 267–272 (2012).
56. F. de Groot and A. Kotani, *Core Level Spectroscopy of Solids, Advances in Condensed Matter Science* (CRC Press, 2008).
57. B. L. Henke, E. M. Gullikson, and J. C. Davis, "X-ray interactions: photoabsorption, scattering, transmission, and reflection at E = 50–30,000 eV, Z = 1–92," At. Data Nucl. Data Tables **54**, 181–342 (1993).
58. L. R. Baker, C.-M. Jiang, S. T. Kelly, J. M. Lucas, J. Vura-Weis, M. K. Gilles, A. P. Alivisatos, and S. R. Leone, "Charge carrier dynamics of photoexcited Co_3O_4 in methanol: extending high harmonic transient absorption spectroscopy to liquid environments," Nano Lett. **14**, 5883–5890 (2014).
59. A. Cavalleri, H. H. W. Chong, S. Fourmaux, T. E. Glover, P. A. Heimann, J. C. Kieffer, B. S. Mun, H. A. Padmore, and R. W. Schoenlein, "Picosecond soft x-ray absorption measurement of the photo-induced insulator-to-metal transition in VO_2," Phys. Rev. B **69**, 153106 (2004).
60. A. Cavalleri, M. Rini, H. H. W. Chong, S. Fourmaux, T. E. Glover, P. A. Heimann, J. C. Kieffer, and R. W. Schoenlein, "Band-selective measurements of electron dynamics in VO_2 using femtosecond near-edge x-ray absorption," Phys. Rev. Lett. **95**, 067405 (2005).
61. D. G. Cahill, H. E. Fischer, T. Klitsner, E. T. Swartz, and R. O. Pohl, "Thermal conductivity of thin films: measurements and understanding," J. Vac. Sci. Technol. A **7**, 1259–1266 (1989).
62. C. Kern, M. Zürch, J. Petschulat, T. Pertsch, B. Kley, T. Käsebier, U. Hübner, and C. Spielmann, "Comparison of femtosecond laser-induced damage on unstructured vs. nano-structured Au-targets," Appl. Phys. A **104**, 15–21 (2011).
63. E. D. Palik, *Handbook of Optical Constants of Solids* (Elsevier, 1997).
64. A. Schiffrin, T. Paasch-Colberg, N. Karpowicz, V. Apalkov, D. Gerster, S. Mühlbrandt, M. Korbman, J. Reichert, M. Schultze, S. Holzner, J. V. Barth, R. Kienberger, R. Ernstorfer, V. S. Yakovlev, M. I. Stockman, and F. Krausz, "Optical-field-induced current in dielectrics," Nature **493**, 70–74 (2012).
65. G. L. Miessler, P. J. Fischer, and D. A. Tarr, *Inorganic Chemistry*, 5th ed. (Prentice-Hall, 2013).
66. N. C. Debnath and A. B. Anderson, "Optical spectra of ferrous and ferric oxides and the passive film: a molecular orbital study," J. Electrochem. Soc. **129**, 2169–2174 (1982).
67. D. M. Sherman and T. D. Waite, "Electronic spectra of Fe^{3+} oxides and oxide hydroxides in the near IR to near UV," Am. Mineral. **70**, 1262–1269 (1985).
68. P. Liao and E. A. Carter, "Optical excitations in hematite (α-Fe_2O_3) via embedded cluster models: a CASPT2 study," J. Phys. Chem. C **115**, 20795–20805 (2011).
69. L. A. Marusak, R. Messier, and W. B. White, "Optical absorption spectrum of hematite, αFe_2O_3 near IR to UV," J. Phys. Chem. Solids **41**, 981–984 (1980).
70. J. Chen, X. Wu, and A. Selloni, "Electronic structure and bonding properties of cobalt oxide in the spinel structure," Phys. Rev. B **83**, 245204 (2011).
71. C. Bressler and M. Chergui, "Molecular structural dynamics probed by ultrafast x-ray absorption spectroscopy," Annu. Rev. Phys. Chem. **61**, 263–282 (2010).
72. L. X. Chen, "Probing transient molecular structures in photochemical processes using laser-initiated time-resolved x-ray absorption spectroscopy," Annu. Rev. Phys. Chem. **56**, 221–254 (2005).
73. E. Stavitski and F. M. F. de Groot, "The CTM4XAS program for EELS and XAS spectral shape analysis of transition metal L edges," Micron **41**, 687–694 (2010).
74. K. Yabana, T. Sugiyama, Y. Shinohara, T. Otobe, and G. F. Bertsch, "Time-dependent density functional theory for strong electromagnetic fields in crystalline solids," Phys. Rev. B **85**, 045134 (2012).
75. S. H. Lin, *Advances in Multi-Photon Processes and Spectroscopy* (World Scientific, 2014).
76. G. Vampa, T. J. Hammond, N. Thiré, B. E. Schmidt, F. Légaré, C. R. McDonald, T. Brabec, and P. B. Corkum, "Linking high harmonics from gases and solids," Nature **522**, 462–464 (2015).
77. C. Spielmann, "Electrons take the fast track through silicon," Science **346**, 1293–1294 (2014).
78. M. Beye, F. Hennies, M. Deppe, E. Suljoti, M. Nagasono, W. Wurth, and A. Föhlisch, "Measurement of the predicted asymmetric closing behaviour of the band gap of silicon using x-ray absorption and emission spectroscopy," New J. Phys. **12**, 043011 (2010).
79. P. D. O. Madelung, "Elements of the IVth group and IV-IV compounds," in *Semiconductors: Data Handbook* (Springer, 2004), pp. 7–70.
80. P. Tangney and S. Fahy, "Density-functional theory approach to ultrafast laser excitation of semiconductors: application to the A_1 phonon in tellurium," Phys. Rev. B **65**, 054302 (2002).